

# Accepted Manuscript

Nodal flexibility and kinematic indeterminacy analyses of symmetric tensegrity structures using orbits of nodes

Yao Chen , Jiayi Yan , Pooya Sareh , Jian Feng

PII: S0020-7403(18)33973-0  
DOI: <https://doi.org/10.1016/j.ijmecsci.2019.02.021>  
Reference: MS 4781



To appear in: *International Journal of Mechanical Sciences*

Received date: 30 November 2018  
Revised date: 11 February 2019  
Accepted date: 15 February 2019

Please cite this article as: Yao Chen , Jiayi Yan , Pooya Sareh , Jian Feng , Nodal flexibility and kinematic indeterminacy analyses of symmetric tensegrity structures using orbits of nodes, *International Journal of Mechanical Sciences* (2019), doi: <https://doi.org/10.1016/j.ijmecsci.2019.02.021>

This is a PDF file of an unedited manuscript that has been accepted for publication. As a service to our customers we are providing this early version of the manuscript. The manuscript will undergo copyediting, typesetting, and review of the resulting proof before it is published in its final form. Please note that during the production process errors may be discovered which could affect the content, and all legal disclaimers that apply to the journal pertain.

**Highlights**

- Nodal flexibility analysis of tensegrity structures is presented.
- Symmetry orbits of nodes and Moore-Penrose inverse are adopted for the proposed approach.
- Distributed kinematic indeterminacy of different nodes can be independently computed.
- Flexibility ellipsoid is introduced to visually characterize nodal flexibility.

ACCEPTED MANUSCRIPT

# Nodal flexibility and kinematic indeterminacy analyses of symmetric tensegrity structures using orbits of nodes

Yao Chen<sup>1\*</sup>, Jiayi Yan<sup>1</sup>, Pooya Sareh<sup>2</sup>, Jian Feng<sup>1</sup>

*1 Key Laboratory of Concrete and Prestressed Concrete Structures of Ministry of Education, and National Prestress Engineering Research Center, Southeast University, Nanjing 211189, China*

*2 Creative Design Engineering Lab, Division of Industrial Design, Faculty of Engineering, University of Liverpool, London Campus, EC2A 1AG, UK*

**Abstract:** A tensegrity structure may undergo large deformations under external loads, resulting in significant impact on its mechanical properties. Therefore, the nodal flexibility analysis of tensegrity structures, that is, analyzing the sensitivity of nodal displacements to external loads and the evaluation of critical nodes, is important in the structural design of tensegrities. Here, we present a numerical method for the symmetry-adapted flexibility analysis and kinematic indeterminacy of tensegrity structures using orbits of nodes and the Moore-Penrose inverse of involved matrices. To evaluate the contribution of each node to the total kinematic indeterminacy of a tensegrity structure, the distributed kinematic indeterminacies associated with the nodes of different orbits are independently computed. A flexibility ellipsoid is introduced to visually characterize the nodal flexibility of tensegrity structures. Several examples of tensegrities with different symmetries are presented to demonstrate the efficiency of the presented method. This method can be applied to the design and analysis of tensegrity structures under external loads, where flexibility ellipsoids are expected to be full and similar and each node is expected to have proper sensitivity to the external loads along different directions.

**Keywords:** flexibility ellipsoid; kinematic indeterminacy; symmetry group; tensegrity; prestress

## 1. Introduction

Unlike most traditional structures, tensegrity structures contain flexible members such as cables or tendons, and generally rely on prestressing in the cables and struts to maintain structural stability [1, 2]. In fact, because of low stiffness, very few of such structural concepts have been built as large-scale space structures [3-5]. A tensegrity structure may experience large deformations under external loads [6, 7], leading to substantial changes in the mechanical properties of the structure. Therefore, the nodal flexibility analysis of tensegrity structures, that is, the study of the sensitivity of nodal displacements to external loads and the identification of critical nodes [8-11], is of great importance in the design and analysis of tensegrity structures.

Flexibility analysis of a structure can indicate potential deformations and basic characteristics of the structure subjected to external loads, which is analogous to stiffness analysis using the tangent stiffness matrix. Thereafter, the evaluation index for the flexibility of the structure can be based on the flexibility matrix [9, 11]. A number of studies have been conducted on the level of the entire structure, to explore the stiffness or flexibility characteristics of prestressed cable-strut structures [1, 11-14]. On the one hand, novel configurations with

---

### Corresponding author:

Yao Chen, Key Laboratory of Concrete and Prestressed Concrete Structures of Ministry of Education, and National Prestress Engineering Research Center, Southeast University, Nanjing 211189, China  
Email: chenyaoyao@seu.edu.cn

desirable structural stiffness can be achieved by the means of form-finding methodologies [15, 16] such as the force density method [17, 18], dynamic relaxation method [19], nonlinear iteration methods [20], finite element method [21, 22], symmetry methods [23-25] and optimization methods [26-29]. On the other hand, force-finding techniques allow a structure to possess desirable stiffness and initial prestress distribution. Existing force-finding methods are generally based on independent self-stress states, integral self-stress states with full symmetry [30, 31], or specific optimization techniques [32, 33].

However, there are a limited number of studies performed on the level of nodes and members, concerning the stiffness or flexibility characteristics of tensegrity structures. Note that the flexibility characteristics of a structure can be described using its nodal flexibilities (i.e., nodal displacement under a unit load) [34]. In fact, as far as a single node is concerned, the involved nodal flexibility analysis can be evaluated from the entries corresponding to the node in the overall flexibility matrix, which is known as the nodal flexibility matrix [8, 35]. The nodal flexibility analysis reveals the influence of external loads on certain nodal displacements, which can be expressed as the sensitivity of nodes to external loads. Ströbel and Singer [34] have found that the incremental displacement of each node of a tension structure can be neatly described as the flexibility ellipsoids for a unit load acting at the same node. Wagner [36] has adopted flexibility ellipsoids to show the three-dimensional deformations of the nodes of cable nets and membrane structures. Recently, Dalilsafaei et al. [37] utilized flexibility ellipsoids to not only find the most flexible directions of slender boom structures, but also improve the bending stiffness of those booms. On the level of members, Shekastehband et al. [38] estimated the sensitivity of tensegrity structures. Chen et al. [39] presented a symmetry method to evaluate the contribution of each member to the static indeterminacy and elastic redundancy of tensegrity structures. Eriksson and Tibert [35] explained the concepts of static and kinematic indeterminacy, and proposed an analytical method for distributed static indeterminacy. Subsequently, Zhou et al. [40] extended the concepts of distributed static indeterminacy and distributed kinematic indeterminacy. Thus, the distributed kinematic indeterminacy of nodes and the nodal flexibility analysis can be effectively adopted for evaluating the importance of different nodes [8].

Nevertheless, for a structure containing a large number of nodes, it becomes computationally expensive to solve the involved flexibility matrices for all the nodes. Conventional methods generally neglect the inherent symmetry [30, 41]. Nevertheless, it has been validated that symmetry analysis can not only simplify the computational process, but also provide useful insights [42-44]. In fact, as most tensegrity structures hold a certain symmetry (e.g., cyclic, dihedral, or cubic symmetry) [24, 25, 30, 39], all nodes and members belong to certain symmetry orbits and remain invariant under symmetry operations. Here, the orbits of nodes will be fully utilized, which means that each symmetry operation would shift one node to coincide with another node on the same orbit [25, 45].

More importantly, because tensegrity structures are generally free-standing, the corresponding tangent stiffness matrices are singular [20, 33]. Then, it is impossible for a tensegrity structure to compute the flexibility matrix from the inverse of the tangent stiffness matrix. Recent studies have pointed out that rigid-body motions can be excluded by deliberately applying appropriate boundary constraints [37, 40]. However, the way in which the constraints are introduced to the structure has a significant effect on the flexibility analysis, and can even disturb the results of the nodal flexibility matrices.

In this study, a numerical method for the symmetry-adapted nodal flexibility analysis and improved distributed kinematic indeterminacy of tensegrity structures is presented. A novel computational scheme for symmetric tensegrities is proposed by considering the inherent symmetry and using orbits of nodes, where every node can be transformed to coincide with another node on the same orbit of nodes under a symmetry operation. To deal with the singular stiffness matrix of a free-standing tensegrity, the Moore-Penrose inverse is introduced for the involved flexibility matrices. To evaluate the contribution of each node to the total kinematic indeterminacy, distributed kinematic indeterminacy values of the nodes of different orbits are independently computed.

Moreover, flexibility ellipsoids are introduced and formulated to visually characterize the nodal flexibility of tensegrity structures.

## 2. Distributed kinematic indeterminacy

### 2.1. Fundamental assumptions

In this study, the following assumptions have been adopted:

- (i) Each cable member is considered to be in tension, and each strut member is subjected to either axial compression or tension.
- (ii) The structure has a proper prestress level to ensure for the linear elastic state.
- (iii) The axial strain of each member is much smaller than the initial length of the member.
- (iv) External loads are applied on the nodes, and the gravity load is not considered.

### 2.2. Distributed kinematic indeterminacy of the nodes of the same orbit

It is well-known that, in the finite element method, the tangent stiffness matrix  $\mathbf{K}_T$  yields a general relationship between incremental forces to incremental displacements from a specific state. That is

$$\mathbf{K}_T \mathbf{d} = \mathbf{p} \quad (1)$$

where  $\mathbf{K}_T$  denotes the tangent stiffness matrix,  $\mathbf{p}$  denotes the incremental force vector, and the vector  $\mathbf{d}$  describes the nodal displacements. For a prestressed structure stating at the initial equilibrium configuration, the tangent stiffness is  $\mathbf{K}_T$  given by

$$\mathbf{K}_T = \mathbf{H}\bar{\mathbf{G}}\mathbf{H}^T + \mathbf{K}_G \quad (2)$$

where  $\mathbf{K}_G$  is the geometric stiffness matrix,  $\mathbf{H}$  is the equilibrium matrix, and the diagonal matrix  $\bar{\mathbf{G}}$  contains the modified axial stiffness of each member [1, 44].

For a kinematically indeterminate structure where the equilibrium matrix  $\mathbf{H}$  has left null space [9, 24, 40], the nodal displacements  $\mathbf{d}$  can be written as

$$\mathbf{d} = \mathbf{M}\boldsymbol{\beta}, \text{ where } \mathbf{H}^T \mathbf{M} = \mathbf{0} \quad (3)$$

In Eq. (3), the matrix  $\mathbf{M}$  includes the basic bases for the internal and independent mechanisms, and its dimension  $m$  is known as the total degree of kinematic indeterminacy (or known as the mobility) [23, 40]. In addition, the coefficient vector  $\boldsymbol{\beta}$  in Eq. (3) can be determined by [40, 46]

$$\boldsymbol{\beta} = (\mathbf{M}^T \mathbf{K}_G \mathbf{M})^{-1} \mathbf{M}^T \mathbf{p} \quad (4)$$

Then, by substituting Eq. (4) into Eq. (3), the nodal displacements  $\mathbf{d}$  can be rewritten as

$$\mathbf{d} = \mathbf{M}(\mathbf{M}^T \mathbf{K}_G \mathbf{M})^{-1} \mathbf{M}^T \mathbf{p} = \mathbf{K}_G^{-1} \boldsymbol{\Phi} \mathbf{p} \quad (5)$$

where the idempotent matrix  $\boldsymbol{\Phi}$  is given by

$$\boldsymbol{\Phi} = \mathbf{K}_G \mathbf{M}(\mathbf{M}^T \mathbf{K}_G \mathbf{M})^{-1} \mathbf{M}^T \quad (6)$$

It is worth noting that the trace of this matrix is equivalent to the total degree of kinematic indeterminacy  $m$ . Zhou et al. [40] have defined the diagonal entries of the matrix  $\boldsymbol{\Phi}$  as the distributed kinematic indeterminacies, which describe kinematic evaluation of a structure from the level of the node and consider the stiffness of the members. This is because these diagonal entries can effectively reveal the contribution of each node to the total kinematic indeterminacy in different directions of the 3D space.

Moreover, as far as the inherent symmetry of a structure is concerned, every node which lies on the same orbit

of symmetry has the same nodal mobility (i.e.,  $\Phi_{ii}$ ). Thus, the distributed kinematic indeterminacy associated with the nodes of an orbit can be independently computed by

$$\boldsymbol{\eta}_j = \overline{\mathbf{K}}_{G_j} \mathbf{M} (\mathbf{M}^T \mathbf{K}_G \mathbf{M})^{-1} \overline{\mathbf{M}}_j^T, \quad j \in [1, \bar{n}] \quad (7)$$

where  $\boldsymbol{\eta}_j$  denotes the distributed kinematic indeterminacy of the nodes of the  $j$ -th orbit, and  $\bar{n}$  is the total number of orbits for the nodes of the structure. In Eq. (7), the matrices  $\overline{\mathbf{K}}_{G_j}$  and  $\overline{\mathbf{M}}_j$  are the sub-matrices of  $\mathbf{K}_G$  and  $\mathbf{M}$  associated with the first node of the  $j$ -th orbit. For a  $d$ -dimensional structure,  $\boldsymbol{\eta}_j$  is a  $d$ -dimensional vector whose entries reveal the kinematic indeterminacy along  $d$  directions. The total degree of kinematic indeterminacy  $m$  can be expressed as

$$m = \sum_{j=1}^{\bar{n}} n_j m_j, \quad \text{and} \quad m_j = \sum_{i=1}^d \boldsymbol{\eta}_{ji} \quad (8)$$

where  $n_j$  is the total number of nodes of the  $j$ -th orbit, and  $m_j$  denotes the nodal mobility for each node of the  $j$ -th orbit.

### 3. Nodal flexibility analysis

#### 3.1. Nodal flexibility matrix

Note that the inverse relation between the nodal displacements  $\mathbf{d}$  and the external forces  $\mathbf{p}$  in the global coordinate system can be obtained from Eq. (1)

$$(\mathbf{K}_T)^{-1} \mathbf{p} = \mathbf{F} \mathbf{p} = \mathbf{d} \quad (9)$$

where the matrix  $\mathbf{F} = (\mathbf{K}_T)^{-1}$  is called as the global flexibility matrix  $\mathbf{F}$ , which denotes the relation between the external loads at a node and the corresponding nodal displacements. For a free-standing tensegrity structure, the flexibility matrix  $\mathbf{F}$  is given by

$$\mathbf{F} = (\mathbf{K}_T)^+ \quad (10)$$

where  $(\mathbf{K}_T)^+$  denotes the Moore-Penrose inverse (a well-known type of matrix pseudoinverse) of the stiffness matrix  $\mathbf{K}_T$  [47], to exclude the trivial effects of rigid-body motions. Importantly, under a specific load condition, the displacement of node  $i$  is fully determined by the involved entries of the global flexibility matrix [34] and is independent of the other entries. In this case, a reduced and nodal flexibility equation can be extracted, which denotes the relationship between the nodal force vector and the nodal displacement vector of the node subjected to an external force. For instance, each node of a 3D tensegrity has  $d=3$  degrees of freedom. Then, the flexibility of node  $i$  is obtained from a  $3 \times 3$  matrix  $\mathbf{F}^i$  expressed by

$$\mathbf{F}^i \mathbf{p}^i = \begin{bmatrix} f_{xx}^i & f_{xy}^i & f_{xz}^i \\ f_{yx}^i & f_{yy}^i & f_{yz}^i \\ f_{zx}^i & f_{zy}^i & f_{zz}^i \end{bmatrix} \begin{bmatrix} p_x^i \\ p_y^i \\ p_z^i \end{bmatrix} = \begin{bmatrix} d_x^i \\ d_y^i \\ d_z^i \end{bmatrix} = \mathbf{d}^i \quad (11)$$

where  $\mathbf{F}^i$  is the nodal flexibility matrix,  $\mathbf{p}^i = [p_x^i \ p_y^i \ p_z^i]^T$  denotes the external loads acting on node  $i$ , and

$\mathbf{d}^i = [d_x^i \ d_y^i \ d_z^i]^T$  represents the nodal displacements along the  $x$ ,  $y$ , and  $z$  directions. It should be noted that the

physical meaning of the entry  $f_{xx}^i$  is the displacement of node  $i$  along the  $x$  direction under the unit load along the  $x$  direction applied to the node, while  $f_{xy}^i$  denotes the corresponding nodal displacement along the  $x$  direction under the unit load along the  $y$  direction applied to the node  $i$ . The other entries in the matrix  $\mathbf{F}^i$  in Eq. (11) can be explained in a similar manner.

In general, the nodal flexibility matrices of a tensegrity structure can be computed from the Moore-Penrose inverse of the tangent stiffness matrix associated with the structure (see Eq. (10)). However, for large-scale tensegrity structures with many nodes and complex geometries, the stiffness matrices are rather large-sized and the inversion is computationally expensive. To avoid such tedious computations, unit loads can be applied to different types of free nodes, according to the physical meaning of the influence coefficients in Eq. (11). Then, the flexibility matrices associated with various nodes can be efficiently established.

### 3.2. Ellipsoid equation associated with nodal flexibility

Based on the Reciprocal theorem of displacement and Eq. (10), the entries of nodal flexibility matrix  $\mathbf{F}^i$  in Eq. (11) satisfy

$$f_{xy}^i = f_{yx}^i, \quad f_{xz}^i = f_{zx}^i, \quad f_{yz}^i = f_{zy}^i \quad (12)$$

Thus, the nodal flexibility matrix  $\mathbf{F}^i$  is a real symmetric matrix. Then, there must be an orthogonal matrix  $\mathbf{V}^i$  that will transform the matrix  $\mathbf{F}^i$  into a diagonal matrix:

$$(\mathbf{V}^i)^{-1} \mathbf{F}^i \mathbf{V}^i = (\mathbf{V}^i)^T \mathbf{F}^i \mathbf{V}^i = \overline{\mathbf{F}}^i \quad (13)$$

where  $\overline{\mathbf{F}}^i$  is the diagonal flexibility matrix of which the diagonal entries are the eigenvalues of the matrix  $\mathbf{F}^i$ . In fact, the orthogonal matrix  $\mathbf{V}^i$  neatly transforms the original nodal flexibility matrix in the global coordinate system into a diagonal flexibility matrix in a certain local coordinate system. In the local coordinate system, the unit load along each local direction  $\xi$ ,  $\eta$ , or  $\zeta$  only induces a nodal displacement along the same direction [8].

Similarly, the external load vector  $\overline{\mathbf{p}}^i$  and nodal displacement vector  $\overline{\mathbf{d}}^i$  of node  $i$  in the local coordinate system can be transformed from those expressed in the global coordinate system:

$$\overline{\mathbf{p}}^i = (\mathbf{V}^i)^T \mathbf{p}^i, \quad \overline{\mathbf{d}}^i = (\mathbf{V}^i)^T \mathbf{d}^i \quad (14)$$

By combining Eq. (13) with Eq. (14), we have

$$\overline{\mathbf{F}}^i \overline{\mathbf{p}}^i = \begin{bmatrix} f_{\xi}^i & 0 & 0 \\ 0 & f_{\eta}^i & 0 \\ 0 & 0 & f_{\zeta}^i \end{bmatrix} \begin{bmatrix} p_{\xi}^i \\ p_{\eta}^i \\ p_{\zeta}^i \end{bmatrix} = \begin{bmatrix} d_{\xi}^i \\ d_{\eta}^i \\ d_{\zeta}^i \end{bmatrix} = \overline{\mathbf{d}}^i \quad (15)$$

where  $f_{\xi}^i$ ,  $f_{\eta}^i$ , and  $f_{\zeta}^i$  respectively denote the influence coefficients along the directions  $\xi$ ,  $\eta$ , and  $\zeta$  of the local coordinate system. The vectors  $\overline{\mathbf{p}}^i = [p_{\xi}^i \ p_{\eta}^i \ p_{\zeta}^i]^T$  and  $\overline{\mathbf{d}}^i = [d_{\xi}^i \ d_{\eta}^i \ d_{\zeta}^i]^T$  are the external load vector and the nodal displacement vector expressed in the local coordinate system.

Because the external load  $\mathbf{p}^i$  acting on the node  $i$  is a unit load, that is  $(p_{\xi}^i)^2 + (p_{\eta}^i)^2 + (p_{\zeta}^i)^2 = 1$ , the

following relationship can be obtained from Eq. (15):

$$\left(\frac{d_{\xi}^i}{f_{\xi}^i}\right)^2 + \left(\frac{d_{\eta}^i}{f_{\eta}^i}\right)^2 + \left(\frac{d_{\zeta}^i}{f_{\zeta}^i}\right)^2 = 1 \quad (16)$$

Eq. (16) is an exact expression of an ellipsoid equation, which is known as the flexibility ellipsoid of node  $i$ . It expresses the changes of nodal displacements under the external load, whereas the lengths of the half-axes  $f_{\xi}^i$ ,  $f_{\eta}^i$ , and  $f_{\zeta}^i$  describe the flexibility of node  $i$  in the local coordinate system. Notably, the nodal flexibility ellipsoid and its ellipsoid equation given in Eq. (16) can reflect the sensitivity of the node and the distribution of nodal sensitivity for the entire structure [36]. Consequently, the critical nodes of the structure can be detected. Moreover, based on the fullness of the flexibility ellipsoid of each node, the sensitivity of the nodes along different directions and under various loads can be evaluated [8].

### 3.3. Flexibility ellipsoids of nodes of same orbit

Conventionally, the origin of the local coordinate system is located at node  $i$ , and thus it is dependent on the specific positions of different nodes. However, the flexibility ellipsoid of each node can be independently evaluated. Moreover, as far as a tensegrity structure with a certain symmetry is concerned, only one node of an orbit is needed to find its nodal flexibility ellipsoid. The others can be effectively obtained using the symmetry of the nodes belonged to the same orbit. This implies that, starting with one node, an independent symmetry operation  $S$  would shift that node to coincide with another node on the same orbit [25, 43, 45].

From the viewpoint of symmetry, a tensegrity structure with  $n$  nodes has  $1 \leq \bar{n} \leq n$  orbits of nodes [39, 41]. Supposing that nodes  $i$  and  $i'$  are located on the same orbit, then we can write

$$\mathbf{p}^{i'} = \mathbf{R}_S^i \mathbf{p}^i, \quad \mathbf{d}^{i'} = \mathbf{R}_S^i \mathbf{d}^i \quad (17)$$

where  $\mathbf{R}_S^i$  is the  $d \times d$  transformation matrix for the symmetry operation  $S$ ,  $\mathbf{p}^{i'}$  is the external load acting on the node  $i'$ , and  $\mathbf{d}^{i'}$  is the nodal displacement for the node  $i'$ . Besides, the orthogonal matrix  $\mathbf{V}^{i'}$  for the node  $i'$  can be expressed as

$$\mathbf{V}^{i'} = \mathbf{R}_S^i \mathbf{V}^i \quad (18)$$

Since linear transformations do not change the eigenvalues of the matrix [42, 44], the flexibility ellipsoid of nodes of the same type remains invariant. The matrix  $\mathbf{V}^{i'}$  in Eq. (18) indicates  $d$  orthogonal axes of the ellipsoid for the node  $i'$  (it becomes an ellipse when  $d=2$ ). Each column of  $\mathbf{V}^{i'}$  is parallel to one of the directions  $f_{\xi}^{i'}$ ,  $f_{\eta}^{i'}$ , or  $f_{\zeta}^{i'}$  in the local coordinate system.

Such a flexibility ellipsoid can visually show the change of the nodal displacement under an external load. In other words, the larger the flexibility value of a node along an axis, the more likely it is to be displaced along this direction. Hence, after evaluating the half-axis lengths of the ellipsoid and the local coordinate system of a typical node of the same orbit, we can quantitatively analyze the most important nodes of the structure and their sensitive directions.

## 4. Illustrative examples

A numerical approach implemented in MATLAB is developed for the nodal flexibility analysis and kinematic indeterminacy evaluation. A number of examples of symmetric tensegrity structures, including 2D tensegrity,

expanded octahedron tensegrity, and cable domes with Geiger and Levy types, will be investigated. All structures are simplified and modeled as a set of weightless struts and cables connected via pin-joints. It is assumed that, the boundary constraints, the main structure, or the surface cover are not considered in the numerical models, although they are potentially involved in a real engineering structure [34, 39]. In the first two examples, the axial stiffness of the cables is  $E_c A_c = 3.238 \times 10^6 \text{ N}$ , and that of the struts is  $E_s A_s = 6.594 \times 10^7 \text{ N}$  [40].

#### 4.1. 2D tensegrity structure with three struts

Figure 1 shows a simple 2D tensegrity structure with three struts and four cables. The length of strut I is  $l_1 = 2\text{m}$ , and that of strut II is  $l_2 = 3\text{m}$ . The angle between the axis lines of cable I and cable II is  $0.75\pi$ , and the angle between the axis lines of cable I and strut II is  $0.25\pi$ .

First-order analysis shows that this structure has  $m = 1$  mechanism mode with lower-order symmetry (see Fig. 1b), and a self-stress state with full symmetry. Although the structure is both kinematically and statically indeterminate, it can be stable after being prestressed. Note that the nominal strain of every cable I is  $\varepsilon = t/E_c A_c = 0.01$ , while those of other members can be uniquely determined using the self-stress state.

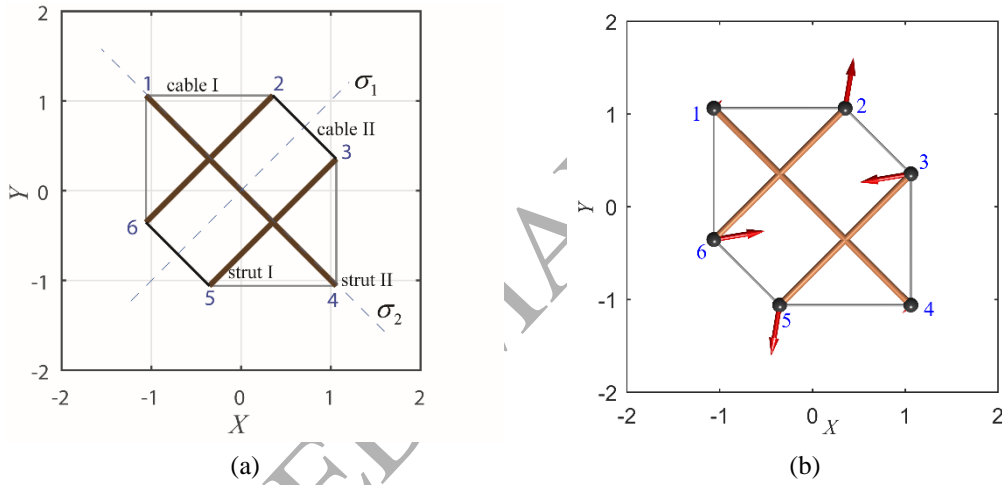


**Figure 1.** A simple 2D tensegrity structure with  $C_{2v}$  symmetry: (a) structural configuration; (b)  $C_2$  symmetric mechanism mode.

This 2D structure is  $C_{2v}$  symmetric (denoted by the Schoenflies notation) according to the cyclic symmetry detection method [48, 49], as it remains unchanged under two rotations and two mirror operations ( $\sigma_1$  and  $\sigma_2$  in Fig. 1a). Six free nodes belong to  $\bar{n} = 2$  distinct symmetry orbits, where the nodes 1 and 4 are on the first orbit ( $n_1 = 2$ ), and the nodes 2, 3, 5, and 6 are on the second orbit ( $n_2 = 4$ ). Because this structure is simple, its nodal flexibility matrices  $\mathbf{F}^i$  can be directly obtained from the Moore-Penrose inverse of the tangent stiffness matrix  $\mathbf{K}_T$  using Eq. (10). Table 1 shows the involved flexibility matrices of typical nodes and the corresponding flexibility matrices expressed in the local coordinate system.

**Table 1.** Nodal flexibility matrices of a 2D tensegrity with  $C_{2v}$  symmetry

Node $i$	Nodal flexibility matrix $\mathbf{F}^i$ ( $\times 10^{-5}$ m/N)	Local matrix $\overline{\mathbf{F}}^i$ ( $\times 10^{-5}$ m/N)	Local coordinate system
1	$\begin{bmatrix} 0.0336 & 0.0227 \\ 0.0227 & 0.0336 \end{bmatrix}$	$\begin{bmatrix} 0.0109 & 0 \\ 0 & 0.0563 \end{bmatrix}$	$\sqrt{2} \times \begin{bmatrix} -0.5 & 0.5 \\ 0.5 & 0.5 \end{bmatrix}$
4	$\begin{bmatrix} 0.0336 & 0.0227 \\ 0.0227 & 0.0336 \end{bmatrix}$	$\begin{bmatrix} 0.0109 & 0 \\ 0 & 0.0563 \end{bmatrix}$	$\sqrt{2} \times \begin{bmatrix} -0.5 & 0.5 \\ 0.5 & 0.5 \end{bmatrix}$
2	$\begin{bmatrix} 0.0248 & 0.1027 \\ 0.1027 & 0.6682 \end{bmatrix}$	$\begin{bmatrix} 0.0088 & 0 \\ 0 & 0.6842 \end{bmatrix}$	$\begin{bmatrix} -0.9881 & 0.1538 \\ 0.1538 & 0.9881 \end{bmatrix}$
6	$\begin{bmatrix} 0.6682 & 0.1027 \\ 0.1027 & 0.0248 \end{bmatrix}$	$\begin{bmatrix} 0.0088 & 0 \\ 0 & 0.6842 \end{bmatrix}$	$\begin{bmatrix} 0.1538 & -0.9881 \\ -0.9881 & -0.1538 \end{bmatrix}$

Table 1 and the inherent symmetry of the structure show that the value of  $f_{\eta}^i = 0.0563 \times 10^{-5}$  m/N ( $i=1, 4$ ), as the nodes 1 and 4 locate at the same symmetry orbit. Similarly, the value of  $f_{\eta}^i = 0.6842 \times 10^{-5}$  m/N ( $i=2, 3, 5, 6$ ), as the nodes 2, 3, 5 and 6 belong to the same symmetry orbit. Figure 2(a) shows the flexibility ellipsoids of this symmetric tensegrity structure, presenting the distributed kinematic indeterminacy of typical nodes 1 and 5 belonging to different symmetry orbits.

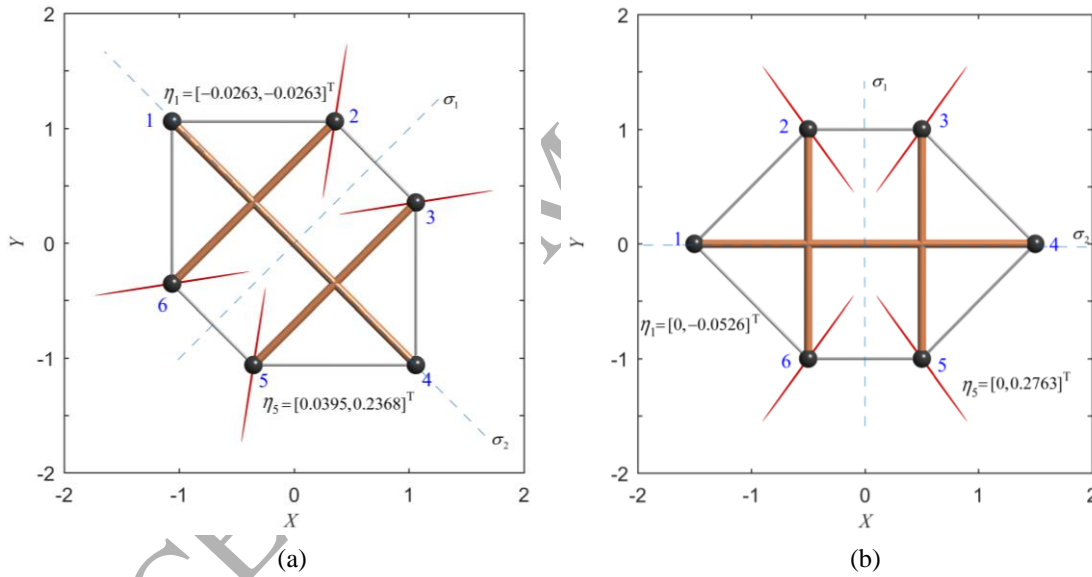


**Figure 2.** Flexibility ellipsoids of a 2D tensegrity with  $C_{2v}$  symmetry: (a) original configuration; (b) rotated by  $0.25\pi$  around the symmetry center.

Note that the flexibility ellipsoids of the structure retain the full symmetry of  $C_{2v}$  group. As can be seen from Table 1 and Fig. 2(a), the local coordinate system of node 1 is obtained by rotating the global coordinate system by  $0.25\pi$ . The flexibility ellipsoids of nodes 1 and 4 are symmetric, as they can be transformed by either a rotation by  $\pi$  or the mirror operation  $\sigma_1$ . Moreover, the local coordinate system of node 2 is along the direction  $[0.1538, 0.9881]^T$  in the global coordinate system, which is the most sensitive direction of node 2 under external loads. In a similar way, node 6 is located on the same orbit as node 2, and its most sensitive direction is along the vector  $[-0.9881, -0.1538]^T$ .

In a similar fashion, an identical structure in a different coordinate system is studied, which is obtained by rotating the original structural configuration by  $0.25\pi$  around the symmetry center, as illustrated in Fig. 2b. Notably, the values of nodal flexibility matrices in the local coordinate system remain invariant, regardless of the rigid-body motions or the change of the coordinate system. Furthermore, as verified by Eq. (19), the sum of distributed kinematic indeterminacy values of each node remains unchanged, although the value along different directions slightly changes.

$$m_1 = -0.0526, \quad m_2 = 0.2763, \quad \text{and} \quad m = -0.0526 \times 2 + 0.2763 \times 4 = 1 \quad (19)$$

#### 4.2. Expanded octahedron tensegrity with $T_h$ symmetry

Figure 3 shows a classic 3D tensegrity structure with  $T_h$  symmetry, known as the expanded octahedron tensegrity [1, 50, 51]. This structure consists of 12 nodes, 24 cables, and 6 struts. As it is based on the expanded octahedron with cubic symmetry, all nodes are from the same symmetry orbit ( $\bar{n} = 1$ ). The length of each strut is  $l_s = 1\text{m}$ , while that of each cable is  $l_c = 0.6124\text{m}$ .

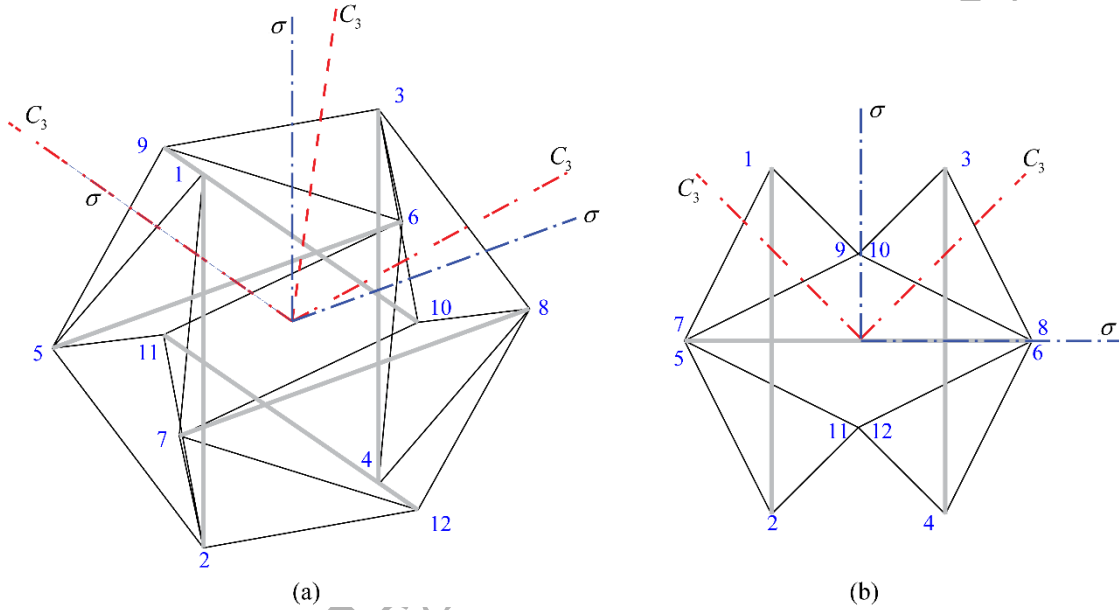


**Figure 3.** Geometric configuration and some of the three-fold symmetry axes of the expanded octahedron tensegrity with  $T_h$  symmetry: (a) perspective view of struts in black solid lines; (b) side view.

First-order analysis shows that the rank of the  $36 \times 30$  equilibrium matrix is 29, and thus the structure has a fully symmetric self-stress state and  $m = 1$  infinitesimal mechanism mode [30, 31, 33]. The corresponding mechanism mode shape is illustrated in Fig. 4(a). To guarantee structural stability, every cable is prestressed to have a nominal strain  $\varepsilon = t/E_c A_c = 0.01$  [1], and the initial prestress of each strut can be determined using the unique self-stress state. After obtaining the  $36 \times 36$  stiffness matrix and the  $36 \times 1$  mechanism mode matrix, we can evaluate the distributed kinematic indeterminacy of the structure by Eqs. (6)-(7). Table 2 gives the corresponding values for all nodes of this tensegrity structure, where the last rows represent the nodal mobility. That is,  $m_i = \eta_{ix} + \eta_{iy} + \eta_{iz}$ , where  $\eta_{ix}$ ,  $\eta_{iy}$  and  $\eta_{iz}$  denote the elements of the distributed kinematic indeterminacy  $\eta_i$  of the node  $i$  along the directions  $x$ ,  $y$  and  $z$ .

**Table 2.** Distributed kinematic indeterminacy of a tensegrity with  $T_h$  symmetry

Node	1	2	3	4	5	6	7	8	9	10	11	12
$\eta_{ix}$	0.083	0.083	0.083	0.083	0.000	0.000	0.000	0.000	0.000	0.000	0.000	0.000
$\eta_{iy}$	0.000	0.000	0.000	0.000	0.083	0.083	0.083	0.083	0.000	0.000	0.000	0.000
$\eta_{iz}$	0.000	0.000	0.000	0.000	0.000	0.000	0.000	0.000	0.083	0.083	0.083	0.083
$m_i$	0.083	0.083	0.083	0.083	0.083	0.083	0.083	0.083	0.083	0.083	0.083	0.083

As listed in Table 2, the sum of all distributed kinematic indeterminacy values is equal to the degree of kinematic indeterminacy,  $\sum_{i=1}^{12} m_i = m = 1$ . It can be noticed that the elements of  $\eta_i$  vary along different directions. However, all nodes have the same nodal mobility (i.e.,  $m_i$ ), as they lie on the same orbit. Moreover, the nodal mobility is independent on certain coordinate systems, although the entries  $\eta_{ix}$ ,  $\eta_{iy}$  and  $\eta_{iz}$  are changed by a different coordinate system.

Moreover, Fig. 4(b) depicts the flexibility ellipsoids of the  $T_h$  symmetric tensegrity. Since this structure is highly symmetric [1, 50], the flexibility ellipsoids of all nodes are equivalent and exhibit the full symmetry of  $T_h$  group. It turns out that the most flexible mode of this tensegrity is in accordance with the infinitesimal mechanism mode shown in Fig. 4(a). In other words, each node is most flexible along the direction that is perpendicular to the axis of the connected strut and lies in the symmetry plane.

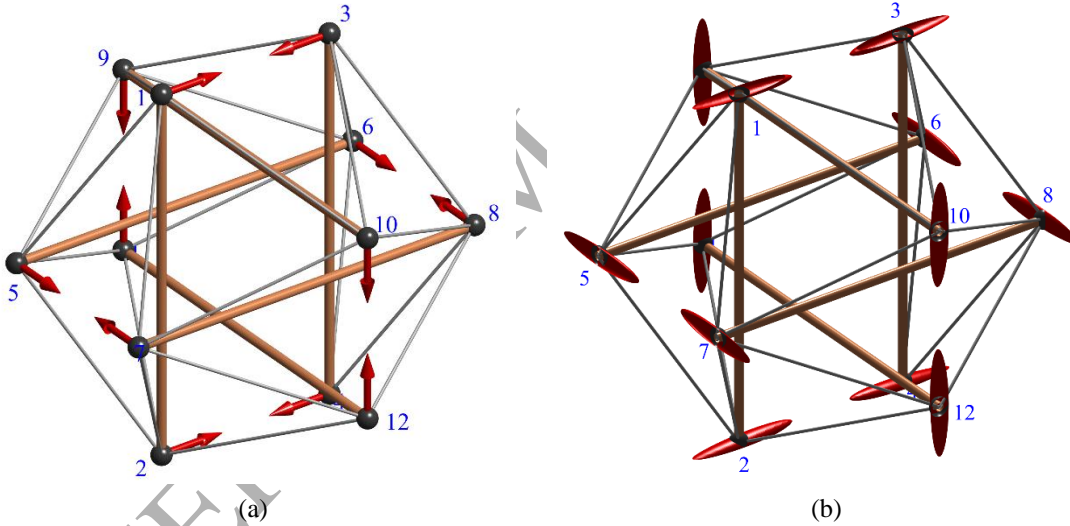


**Figure 4.** Numerical results for the expanded octahedron tensegrity with  $T_h$  symmetry: (a) the internal mechanism mode; (b) the flexibility ellipsoid of each node.

On the other hand, we study how the nodal flexibility of the structure changes as the prestress level increases, described by the nominal strain  $\varepsilon = t/E_c A_c$ . Nominal results for the nodal flexibility and a typical flexibility ellipsoid with  $0 \leq \varepsilon \leq 0.06$  are given in Fig. 5. In fact, a value of the nominal strain  $\varepsilon \geq 0.03$  may be very large in these circumstances and would correspond to a cable member being prestressed close to yield [1]. Here, the yield of members and buckling of compression struts are not considered [52, 53].

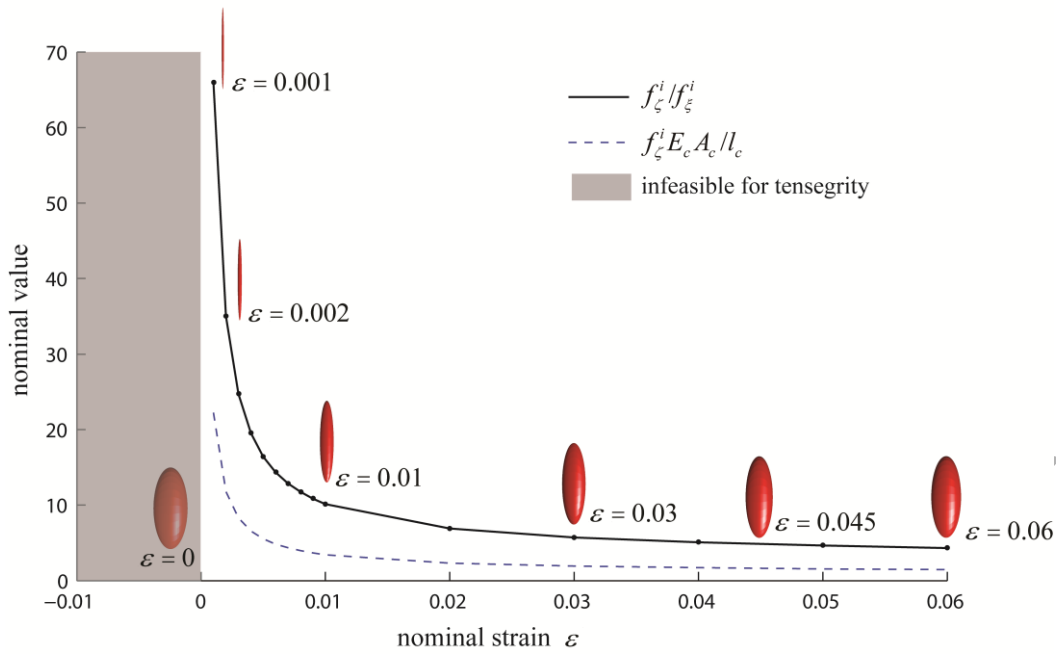


**Figure 5.** Nodal flexibility of the  $T_h$  symmetric tensegrity for a varying prestress level.

Figure 5 shows that the nodal flexibility of tensegrity structures depends on not only the geometric configuration and material properties of the structure, but also on the prestress level of the members. As the prestress level increases, the flexibility ellipsoid becomes fuller and larger, where the values and the unevenness of nodal flexibility along the sensitive directions are significantly reduced. It should be noted that the results in Fig. 5 are not feasible for  $\varepsilon \leq 0$ , as the cables have to be in tension to guarantee stability for the structure.

#### 4.3. Cable domes with $C_{8v}$ symmetry

Figure 6 shows two classic cable domes of diameter 48m [54, 55]. The structures shown in Fig. 6(a) or Fig. 6(b) are assumed to keep  $C_{8v}$  symmetric, and have eight rotations along the 8-fold symmetry axis as well as eight reflections. Each structure consists of 26 pin-joints lying on  $\bar{n} = 5$  orbits, and a total of 8 boundary nodes of orbit 5 are constrained along three directions. The nodes of orbit 4 (or orbit 3) are on the same circle with a radius of 32m, and they are connected to the hoop cables. The heights of struts S1 and S2 are 9.238m and 8.574m, respectively [54].

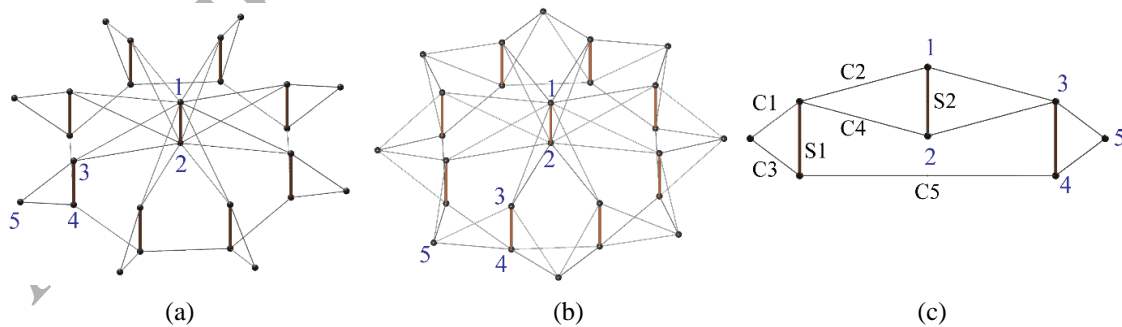


**Figure 6.** Geometric configurations and orbits of nodes of  $C_{8v}$  symmetric cable domes: (a) Geiger type; (b) Levy type; (c) different types of nodes and members illustrated in a symmetry plane.

The cable dome of the Geiger type shown in Fig. 6(a) consists of 9 struts and 40 cables, while the cable dome of the Levy type depicted in Fig. 6(b) consists of 9 struts and 56 cables. As illustrated in Fig. 6(c), all the members can be divided into seven types because of the  $C_{8v}$  symmetry. The initial prestresses ( $P$ ) and lengths ( $l$ )

for different types of members are listed in Table 3 [54]. Each cable is a tendon with a diameter of 50mm, and each strut is a pipe with an outer diameter of 245mm and a thickness of 10mm. The elastic modulus of every member is  $E_c = E_s = 2.1 \times 10^5 \text{ MPa}$ .

**Table 3.** Initial prestresses and lengths for different types of members

Structure	Member type	Cable					Strut	
		C1	C2	C3	C4	C5	S1	S2
Geiger type	$l$ (m)	16.5644	16.5644	9.2377	9.2377	12.2459	9.2380	8.5740
	$P$ (kN)	1000.00	1000.00	2230.74	2230.74	2524.39	-1115.41	-2070.56
Levy type	$l$ (m)	16.5644	16.5644	11.9915	11.9915	12.2459	9.2380	8.5740
	$P$ (kN)	1000.00	1000.00	1876.40	1876.40	2524.39	-1445.57	-2070.56

Based on the first-order analysis, the number of mechanism modes of the structures,  $m$ , is computed. For the Levy cable dome, the rank of the  $54 \times 65$  equilibrium matrix has full rank, and the mobility is  $m = 18 \times 3 - 54 = 0$ . On the contrary, the  $54 \times 49$  equilibrium matrix of the Geiger cable dome is singular with rank 43, and thus  $m = 18 \times 3 - 43 = 11$ . Hence, the nodal mobility for different orbits of nodes should be evaluated using Eqs. (7)-(8). It is validated that

$$m = \sum_{j=1}^{\bar{n}} n_j m_j = m_1 + m_2 + 8m_3 + 8m_4 = 11 \quad (20)$$

where

$$m_1 = 0, \quad m_2 = 0, \quad m_3 = 1.125, \quad m_4 = 0.25 \quad (21)$$

Eq. (21) indicates that the nodes of orbits 3 and 4 are more likely to be mobile, compared with those of orbits 1 and 2. During the nodal flexibility analysis, the nodes of orbit 3 need to be further concerned.

Recall that inherent symmetry considerations in structural analysis can simplify the computational process, and obtain useful insights [42-44, 56, 57]. Because of the inherent symmetry of the structure, only four nodes from orbits 1, 2, 3, and 4 are considered to perform the nodal flexibility analysis. Then, after applying a series of symmetry operations on the nodes of the same orbit [33, 45], the nodal flexibility ellipsoids for the entire structure can be obtained, as shown in Fig. 7 and Fig. 8.

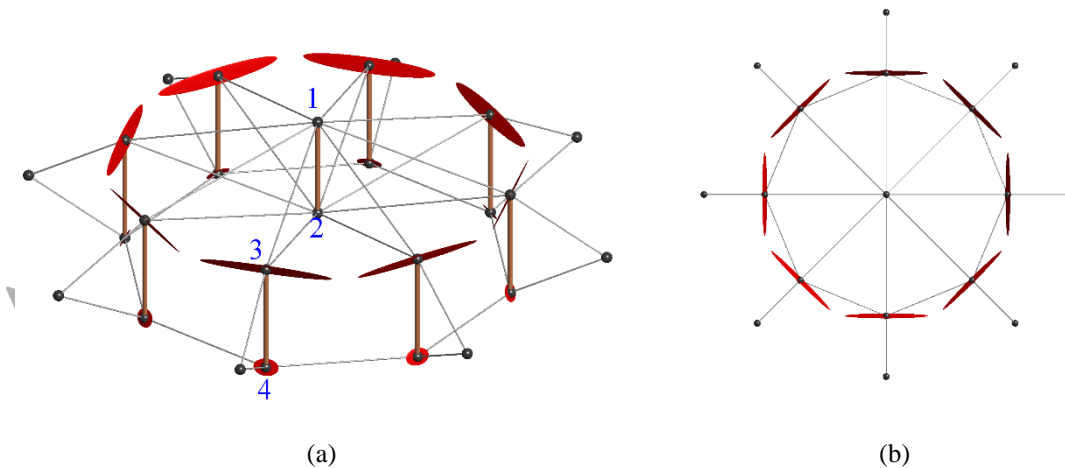


**Figure 7.** Flexibility ellipsoids of a  $C_{8v}$  symmetric cable dome of Geiger type: (a) 3D view; (b) plan view.

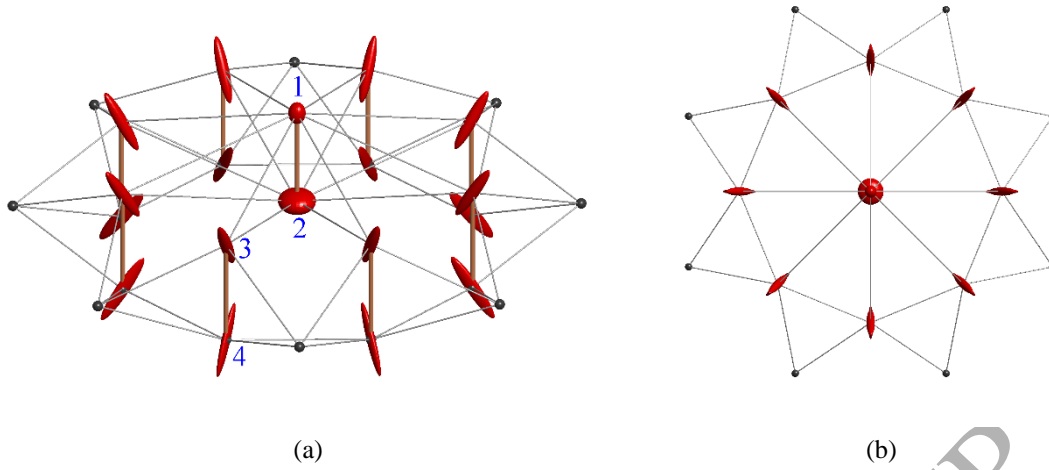


**Figure 8.** Flexibility ellipsoids of a  $C_{8v}$  symmetric cable dome of Levy type: (a) 3D view; (b) plan view.

It can be noticed that the flexibility ellipsoids of both nodes 1 and 2 are small, and they are generally distributed in the plane perpendicular to the axis of the strut S2. As shown in Fig. 7, each node of orbit 3 of the Geiger cable dome is most flexible along the direction perpendicular to the plane on which the cables C1, C2, and C4 and the strut S1 lie. This is because the node is connected to all the adjacent members in a plane, and its out-of-plane stiffness is rather weak. Notably, it is in agreement with the result of the nodal mobility analysis obtained from Eq. (21). The node of orbit 3 of the Geiger cable dome is stiff along the axis of the adjacent cable C1, as the member C1 is connected to a fixed node. Similarly, each node of orbit 4 is stiff along the axis of the adjacent cable C2.

Although the configurations and symmetries of the Levy cable dome and the Geiger cable dome are similar, the flexibility ellipsoids of the nodes of orbits 3 and 4 for the two structures are significantly different. For comparisons, Table 4 gives the flexibility values of different orbits of nodes for the two  $C_{8v}$  symmetric cable domes.

**Table 4.** Flexibility values of different orbits of nodes for the  $C_{8v}$  symmetric cable domes ( $\times l_{C1}/E_c A_c$ )

Geiger	$f_{\xi}^i$	$f_{\eta}^i$	$f_{\zeta}^i$	Levy	$f_{\xi}^i$	$f_{\eta}^i$	$f_{\zeta}^i$
Orbit 1	1.215	1.277	1.277	Orbit 1	0.891	0.891	1.176
Orbit 2	1.271	6.602	6.602	Orbit 2	1.217	1.917	1.917
Orbit 3	0.450	13.226	110.530	Orbit 3	0.616	0.638	3.488
Orbit 4	0.534	13.970	20.876	Orbit 4	0.390	0.770	3.901

As shown in Fig. 8 and Table 4, the flexibility of the Levy cable dome is relatively uniform compared to that of the Geiger cable dome. For the Geiger cable dome, the ratio of the maximum flexibility value to the minimum one is  $f_{\zeta}^i / f_{\xi}^i = 245.62$ . For the Levy cable dome, it has a significant reduction in the value of  $f_{\zeta}^i / f_{\xi}^i$ , which is no more than 10. Importantly, the out-of-plane stiffness of the nodes of orbits 3 and 4 are improved, as the flexibility values of the Levy cable dome are significantly reduced along different directions.

Compared with the Geiger cable dome, the Levy cable dome exhibits a reduced flexibility along the ring direction, which enhances the ability of the dome structure to resist horizontal loads. Both structures are stiff at the end nodes of the central strut S2. Moreover, the nodes of orbits 3 and 4, which are connected to the struts S1, are very flexible along the directions perpendicular to the axes of tension cables C1 and C2. Therefore, the

cables C1 and C2 have a significant influence on the nodal flexibility of the symmetric cable domes.

## 5. Conclusions

This study aimed to exploit the symmetry orbits of nodes and the Moore-Penrose inverse of certain matrices for the kinematic indeterminacy evaluation and the nodal flexibility analysis of symmetric tensegrity structures. Considering nodes belonging to different symmetry orbits, the nodal mobility and flexibility ellipsoids were evaluated to respectively describe the kinematic indeterminacy and flexibility of a structure. The stiffness of tensegrity structures with various symmetry groups were evaluated. Flexible nodes and principal flexibility directions were effectively detected, and the stiffness effects of different prestress levels and structural configurations were discussed. The proposed method can provide insight into the geometric design and flexibility analysis of tensegrity structures for engineering applications.

The efficiency of the proposed method was verified through three examples of tensegrity structures, including a 2D tensegrity with  $C_{2v}$  symmetry, a 3D expanded octahedron tensegrity with  $T_h$  symmetry, and the Geiger and Levy cable domes with  $C_{8v}$  symmetry. We demonstrated that each orbit of nodes has a specific contribution to the total kinematic indeterminacy, which varies in a different coordinate system. However, the sum of distributed kinematic indeterminacy values for each node remains to be the number of internal mechanism modes. Moreover, the flexibility ellipsoids of nodes retain full symmetry, which visually characterize the flexibility of the structures. More importantly, they are approximations of the infinitesimal mechanism modes, and become much fuller and larger with increasing the prestress level. The nodes of the same orbit have poor stiffness along the direction perpendicular to the axis of adjacent members. Future work will focus on the effect of potential slack or rupture of members on the nodal flexibility and symmetry breaking of tensegrity structures.

## Acknowledgement

This research has been supported by the National Natural Science Foundation of China (Grant No. 51508089 and No. 51578133), and the Fundamental Research Funds for the Central Universities. The first author would like to acknowledge financial support from the Alexander von Humboldt-Foundation for his visiting research at Max-Planck-Institut für Eisenforschung GmbH, Germany. The authors are grateful to the anonymous reviewers for their valuable comments.

## References

- [1] Guest SD. The stiffness of tensegrity structures. *IMA Journal of Applied Mathematics*. 2011; 76: 57-66.
- [2] Skelton RE, de Oliveira MC. *Tensegrity Systems*: Springer, 2009.
- [3] Amendola A, Hernandez-Nava E, Goodall R, Todd I, Skelton RE, Fraternali F. On the additive manufacturing, post-tensioning and testing of bi-material tensegrity structures. *Composite Structures*. 2015; 131: 66-71.
- [4] Ali N, Rhode-Barbarigos L, Albi A, Smith I. Design optimization and dynamic analysis of a tensegrity-based footbridge. *Engineering Structures*. 2010; 32: 3650-9.
- [5] Juan SH, Mirats Tur J. Tensegrity frameworks: Static analysis review. *Mechanism and Machine Theory*. 2008; 43: 859-81.
- [6] Rhode-Barbarigos L, Hadj Ali NB, Motro R, Smith IFC. Designing tensegrity modules for pedestrian bridges. *Engineering Structures*. 2010; 32: 1158-67.
- [7] Dubé JF, Angellier N, Crosnier B. Comparison between experimental tests and numerical simulations carried out on a tensegrity minigrad. *Engineering Structures*. 2008; 30: 1905-12.
- [8] Du G. Flexibility analysis of cable and strut tension structures. Shanghai Jiaotong University; 2008.
- [9] Pellegrino S, Kwan A, Vanheerden TF. Reduction of equilibrium, compatibility and flexibility matrices, in

- the force method. *International Journal for Numerical Methods in Engineering*. 1992; 35: 1219-36.
- [10] Amendola A, Carpentieri G, de Oliveira M, Skelton RE, Fraternali F. Experimental investigation of the softening-stiffening response of tensegrity prisms under compressive loading. *Composite Structures*. 2014; 117: 234-43.
- [11] Hanaor A. Prestressed pin-jointed structures-Flexibility analysis and prestress design. *Computers & Structures*. 1988; 28: 757-69.
- [12] Abadi BNR, Shekarforoush SMM, Mahzoon M, Farid M. Kinematic, stiffness, and dynamic analyses of a compliant tensegrity mechanism. *Journal of Mechanisms & Robotics*. 2014; 6: 41001.
- [13] Sultan C. Stiffness formulations and necessary and sufficient conditions for exponential stability of prestressable structures. *International Journal of Solids and Structures*. 2013; 50: 2180-95.
- [14] Hanaor A. Double-layer tensegrity grids: static load response. Part II: Experimental study. *Journal of Structural Engineering*. 1991; 117: 1675-84.
- [15] Masic M, Skelton RE, Gill PE. Algebraic tensegrity form-finding. *International Journal of Solids and Structures*. 2005; 42: 4833-58.
- [16] Tibert AG, Pellegrino S. Review of form-finding methods for tensegrity structures. *International Journal of Space Structures*. 2003; 18: 209-23.
- [17] Nishimura Y, Murakami H. Initial shape-finding and modal analyses of cyclic frustum tensegrity modules. *Computer Methods in Applied Mechanics and Engineering*. 2001; 190: 5795-818.
- [18] Zhang JY, Ohsaki M. Adaptive force density method for form-finding problem of tensegrity structures. *International Journal of Solids and Structures*. 2006; 43: 5658-73.
- [19] Zhang L, Maurin B, Motro R. Form-finding of nonregular tensegrity systems. *Journal of Structural Engineering*. 2006; 132: 1435-40.
- [20] Zhang L, Li Y, Cao Y, Feng X. Stiffness matrix based form-finding method of tensegrity structures. *Engineering Structures*. 2014; 58: 36-48.
- [21] Pagitz M, Mirats Tur JM. Finite element based form-finding algorithm for tensegrity structures. *International Journal of Solids and Structures*. 2009; 46: 3235-40.
- [22] Gasparini D, Klinka KK, Arcaro VF. A finite element for form-finding and static analysis of tensegrity structures. *Journal of Mechanics of Materials and Structures*. 2011; 6: 1239-53.
- [23] Chen Y, Sun Q, Feng J. Group-theoretical form-finding of cable-strut structures based on irreducible representations for rigid-body translations. *International Journal of Mechanical Sciences*, 2018, 144: 205-215.
- [24] Zhang JY, Guest SD, Ohsaki M. Symmetric prismatic tensegrity structures. Part I: Configuration and stability. *International Journal of Solids and Structures*. 2009; 46: 1-14.
- [25] Sareh P, Guest SD. Designing symmetric derivatives of the Miura-ori. *Advances in Architectural Geometry*. 2014; 233-241.
- [26] Lee S, Lee J. A novel method for topology design of tensegrity structures. *Composite Structures*. 2016; 152: 11-9.
- [27] Lee S, Woo B, Lee J. Self-stress design of tensegrity grid structures using genetic algorithm. *International Journal of Mechanical Sciences*. 2014; 79: 38-46.
- [28] Chen Y, Feng J, Wu Y. Novel form-finding of tensegrity structures using ant colony systems. *Journal of Mechanisms and Robotics-Transactions of the ASME*. 2012; 4: 031001.
- [29] Koohestani K. Form-finding of tensegrity structures via genetic algorithm. *International Journal of Solids and Structures*. 2012; 49: 739-47.
- [30] Chen Y, Feng J, Ma R, Zhang Y. Efficient symmetry method for calculating integral prestress modes of statically indeterminate cable-strut structures. *Journal of Structural Engineering*. 2015; 141: 04014240.

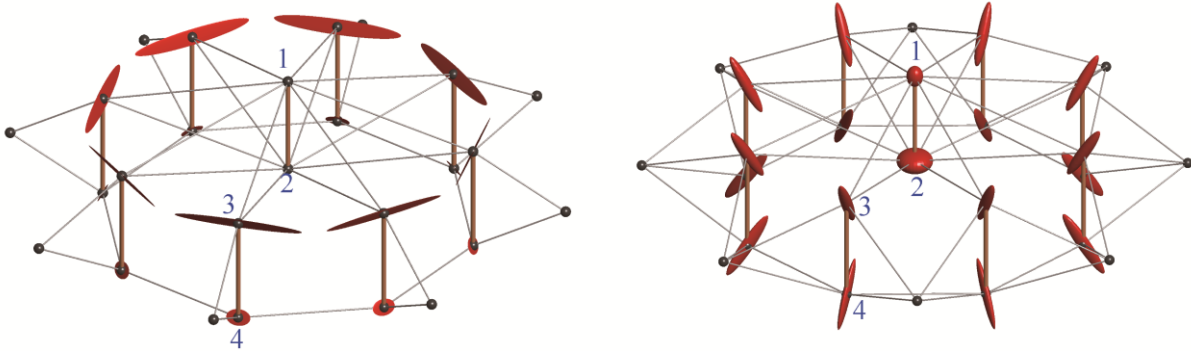
- [31] Yuan XF, Dong SL. Integral feasible prestress of cable domes. *Computers & Structures*. 2003; 81: 2111-9.
- [32] Xu X, Luo YZ. Force finding of tensegrity systems using simulated annealing algorithm. *Journal of Structural Engineering*. 2010; 136: 1027-31.
- [33] Zhang P, Feng J. Initial prestress design and optimization of tensegrity systems based on symmetry and stiffness. *International Journal of Solids and Structures*. 2017; 106: 68-90.
- [34] Ströbel D, Singer P. Recent Developments in the Computational Modelling of Textile Membranes and Inflatable Structures. *Textile Composites and Inflatable Structures II: Springer Netherlands*; 2008, 253-66.
- [35] Eriksson A, Tibert AG. Redundant and force-differentiated systems in engineering and nature. *Computer Methods in Applied Mechanics & Engineering*. 2006; 195: 5437-53.
- [36] Wagner R. *On the Design Process of Tensile Structures: Springer Netherlands*, 2005.
- [37] Dalilsafaei S, Eriksson A, Tibert G. Improving bending stiffness of tensegrity booms. *International Journal of Space Structures*. 2012; 27: 117-29.
- [38] Shekastehband B, Abedi K, Chenaghloou MR. Sensitivity analysis of tensegrity systems due to member loss. *Journal of Constructional Steel Research*. 2011; 67: 1325-40.
- [39] Chen Y, Feng J, Lv H, Sun Q. Symmetry representations and elastic redundancy for members of tensegrity structures. *Composite Structures*. 2018; 203: 672-80.
- [40] Zhou JY, Chen WJ, Zhao B, Qiu ZY, Dong SL. Distributed indeterminacy evaluation of cable-strut structures: formulations and applications. *Journal of Zhejiang University Science A*. 2015; 16: 737-48.
- [41] Kangwai RD, Guest SD, Pellegrino S. An introduction to the analysis of symmetric structures. *Computers & Structures*. 1999; 71: 671-88.
- [42] Zingoni A. Group-theoretic exploitations of symmetry in computational solid and structural mechanics. *International Journal for Numerical Methods in Engineering*. 2009; 79: 253-89.
- [43] Kaveh A. *Optimal Analysis of Structures by Concepts of Symmetry and Regularity: Springer*, 2013.
- [44] Chen Y, Feng J. Generalized eigenvalue analysis of symmetric prestressed structures using group theory. *Journal of Computing in Civil Engineering*. 2012; 26: 488-97.
- [45] Chen Y, Guest SD, Fowler PW, Feng J. Two-orbit switch-pitch structures. *Journal of the International Association for Shell and Spatial Structures*. 2012; 53: 157-62.
- [46] Calladine CR, Pellegrino S. First-order infinitesimal mechanisms. *International Journal of Solids and Structures*. 1991; 27: 505-15.
- [47] Chen Y, Feng J. Efficient method for Moore-Penrose inverse problems involving symmetric structures based on group theory. *Journal of Computing in Civil Engineering*. 2014; 28: 182-90.
- [48] Chen Y, Sareh P, Feng J, Sun Q. A computational method for automated detection of engineering structures with cyclic symmetries. *Computers & Structures*. 2017; 191: 153-164.
- [49] Chen Y, Feng J. Group-theoretic exploitations of symmetry in novel prestressed structures. *Symmetry-Basel*, 2018; 10: 229.
- [50] Estrada GG, Bungartz HJ, Mohrdieck C. Numerical form-finding of tensegrity structures. *International Journal of Solids and Structures*. 2006; 43: 6855-68.
- [51] Xu X, Luo Y. Multistable tensegrity structures. *Journal of Structural Engineering*. 2011; 137: 117-23.
- [52] Chen Y, Sun Q, Feng J. Stiffness degradation of prestressed cable-strut structures observed from variations of lower frequencies. *Acta Mechanica*. 2018; 229: 3319-32.
- [53] Shekastehband B, Abedi K, Dianat N, Chenaghloou MR. Experimental and numerical studies on the collapse behavior of tensegrity systems considering cable rupture and strut collapse with snap-through. *International Journal of Non-Linear Mechanics*. 2012; 47: 751-68.
- [54] Xi Y, Xi Z, Qin WH. Form-finding of cable domes by simplified force density method. *Proceedings of the Institution of Civil Engineers - Structures and Buildings*. 2011; 164: 181-95.

- [55] Levy MP, Jing TF. Floating saddle connections for the Georgia Dome, USA. *Structural Engineering International*. 1994; 4: 148-50.
- [56] Eriksson A, Nordmark A. Symmetry aspects in stability investigations for thin membranes. *Computational Mechanics*. 2016; 58: 747-767.
- [57] Harth P, Michelberger P. Determination of loads in quasi-symmetric structure with symmetry components. *Engineering Structures*. 2016; 123: 395-407.

ACCEPTED MANUSCRIPT

## Graphical Abstract

- ✓ Nodal flexibility analysis of tensegrity structures is presented.
- ✓ Symmetry orbits of nodes and Moore-Penrose inverse are adopted for the proposed approach.
- ✓ Distributed kinematic indeterminacy of different nodes can be independently computed.
- ✓ Flexibility ellipsoid is introduced to visually characterize nodal flexibility.



ACCEPTED MANUSCRIPT